Continuous monitoring of fluvial dike breaching by a Laser Profilometry Technique

I. Rifai[1], V. Schmitz[2], S. Erpicum[2], P. Archambeau[2], D. Violeau[3,4], M. Pirotton[2], B. Dewals[2], and K. El Kadi Abderrezzak[3,4]

[1]Egis, Saint-Quentin-en-Yvelines, France.

[2]University of Liege (ULiège), Research Group of Hydraulics in Environmental and Civil Engineering (HECE), Liège, Belgium.

[3]EDF R&D, National Laboratory for Hydraulics and Environment, Chatou, France.

[4]Saint Venant Laboratory for Hydraulics, Chatou, France.

Corresponding authors: Ismail Rifai (ismail.rifai@egis.fr), Kamal El kadi Abderrezzak (kamal.El-kadi-abderrezzak@edf.fr)

Key Points:

- A non-intrusive, high resolution Laser Profilometry Technique has been developed for continuously monitoring the three dimensional breach shape in dike breaching experiments.
- The capabilities of the Laser Profilometry Technique have been assessed based on dedicated laboratory tests.
- Reliable, time-resolved database of the evolving dike geometry has been collected for testing the accuracy of conceptual or detailed numerical models simulating dike breaching

ABSTRACT

A non-intrusive, high resolution Laser Profilometry Technique (LPT) has been developed for continuous monitoring of the three dimensional (3D) evolving breach in laboratory models of non-cohesive fluvial dikes. This simple and low cost setup consists of a commercial digital video camera and a sweeping red diode 30 mW laser projecting a sheet over the dike. The 2D image coordinates of each deformed laser profile incident on the dike are transformed into 3D object coordinates using the Direct Linear Transformation algorithm. All 3D object coordinates computed over a laser sweeping cycle are merged to generate a cloud of points describing the instantaneous surface. The DLT-based image processing algorithm uses control points and reference axes, so that no prior knowledge is needed on the position, orientation and intrinsic characteristics of the camera, nor on the laser position. Because the dike is partially submerged, ad hoc refraction correction has been developed. Algorithms and instructions for the implementation of the LPT are provided. Reconstructions of a dike geometry with the LPT and with a commercial laser scanner are compared in dry conditions. Using rigid dike geometries, the repeatability of the measurements, the refraction correction, and the dike reconstruction have been evaluated for submerged conditions. Two laboratory studies of evolving fluvial dike breaching due to flow overtopping have been conducted to demonstrate the LPT capabilities and accuracy. The LPT has advantages in terms of flexibility and spatiotemporal resolution, but high turbidity and water surface waves may lead to inaccurate geometry reconstructions.

Keywords: Breach, fluvial Dike, Laboratory experiments, Laser Profilometry Technique, Refraction, 3D geometry reconstructions.

1 INTRODUCTION

Earthen dam or dike (i.e., levee) breaching induced by flow overtopping combines complex interactions between water, soil and structure. Dike breaching is a challenging concern both from the perspective of the scientific issues that are involved (e.g., physical processes, monitoring, numerical modelling) and for the practical consequences of the induced floods (e.g., casualties, damage). The knowledge of the processes involved in breach expansion still calls for further research efforts (Frank, 2016; Rifai *et al.*, 2017, 2018), and despite some advances (e.g., Kakinuma and Shimizu, 2014; Dewals *et al.*, 2018; Onda *et al*., 2019; Dazzi *et al*., 2019; Amaral *et al*., 2020) the current status of dike breaching numerical modelling remains unsatisfactory. The breach development is poorly represented and large uncertainties prevail in the numerical results (Volz *et al*., 2017; Elalfy *et al*., 2018), contrasting with the needs of robust tools for the design of flood hazard maps, emergency plans and mitigation measures.

Characterization of real-world dike failure events remains limited because monitoring is hardly feasible for safety reasons. Investigation of dike breaching *via* experimental modeling is recommended (Schmocker and Hager, 2012; Tabrizi *et al*., 2015) for understanding and quantification of the physical processes. Additionally, well documented, reliable time-resolved, three dimensional (3D) measurements of the evolving dike geometry are essential for the development, calibration, and validation of numerical models (El kadi Abderrezza *et al*., 2016).

Typically, experiments on dike breaching due to overtopping flows focus on studying the flow-soil interactions and sediment transport features (Morris *et al*., 2007; Rifai *et al*., 2016; Frank and Hager, 2016). Studying such processes requires advanced monitoring of: (i) flow characteristics, including in the breach vicinity, at high spatial and temporal resolutions; (ii) dike structure in terms of its integrity, breaching, and/or responses to other stresses, and (iii) processes at the flow-structure interface, such as surface erosion, washout and infiltration.

This paper presents the development and implementation of the Laser Profilometry Technique (LPT), a rapid, non-intrusive, continuous high resolution method for monitoring the 3D breach geometry evolution due to flow overtopping. The development of this method takes part of a broader laboratory research work investigating *fluvial dike* breaching, with a detailed insight into the breach development under various flow and channel configurations as well as dike materials (Rifai *et al*., 2017, 2018, 2019a, 2020). Note that part of the complexity of the breach monitoring stems from the considered *fluvial dike* configuration (i.e., the breached structure is located on the *side* of a main channel, Figure 1) leading to asymmetric breaches, which contrasts with the breaching of an *embankment dam* (i.e., the breached structure is normal to the main channel).

The paper is organized as follows: Section 2 presents a brief review of monitoring methods for bed topography changes in similar applications, with a focus on their transferability to fluvial dike breaching experiments. In Section 3, the principle and implementation of the Laser Profilometry Technique are detailed. The test results and error assessment are analyzed and discussed in Section 4, followed by concluding remarks and outlooks in Section 5.

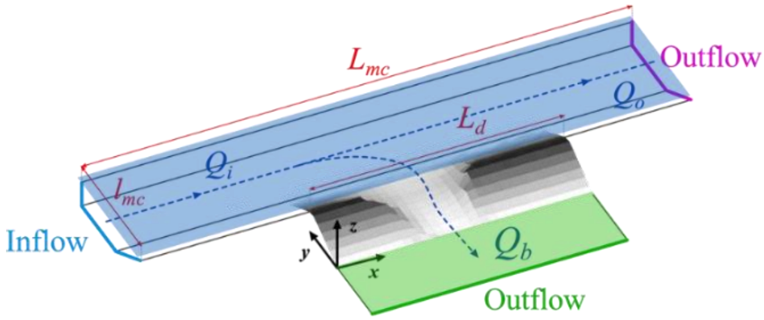

Figure 1. Fluvial dike configuration. The breached dike is in grey, the main channel in blue and the green area is the floodplain. Q_i, Q_o and Q_b refer to channel inflow discharge, channel outflow discharge and breach discharge, respectively. L_{mc}, l_{mc} and L_d are main channel length, main channel width and length of the erodible dike.

2 MONITORING OF BED EVOLUTION IN HYDRAULIC EXPERIMENTS

Broadly, the ability to track evolving fluvial topographies, including in subaqueous conditions, is a matter of interest in various research fields, such as hydro- and geo-morphodynamics (e.g., Bailly *et al.*, 2010; Hung and Capart, 2013; El kadi Abderrezzak *et al.*, 2014). Digital photogrammetry, acceleration sensors, total stations, Global Positioning System (GPS), airborne LIDAR, and Terrestrial Laser Scanning (TLS) have been widely used for topographic data collection in field studies under dry and, to some extent, underwater conditions (Lane, 2000; Brasington *et al.*, 2012; Bouratsis *et al.*, 2013; Smith and Vericat, 2014; Massot-Campos and Oliver-Codina, 2015). However, applying some of these methods during mobile-bed flume experiments remains questionable because of their insufficient measurement accuracy (Friedl *et al.*, 2018), i.e., the level of detail of interest is finer than the accuracy of equipment. Furthermore, when the evolving geometry is submerged, intrusive techniques, such as gauges, probe sensors, thermistors and accelerometers (Jandora and Říha, 2008; Shimada *et al*. 2010, Elalfy *et al*., 2018) are not suitable because they alter the flow field and/or the dike geometry, and therefore the nature of the phenomenon and degree of bed geometry changes.

Remote or non-intrusive techniques are particularly appealing for monitoring the 3D bed topography evolution of an erodible boundary (Smith *et al.*, 2014; Morgan *et al.*, 2017), as the physical processes are presumably unaltered by the instrumentation devices. Among these methods, imagery based techniques have become readily available due to recent advances in digital imaging and processing capabilities (Tal *et al.*, 2012; Chourasiya *et al.*, 2017). In dam breaching induced by flow overtopping over the whole breach crest (i.e., plane erosion), a side view through a glass wall is sufficient to monitor continuously the breach formation through the water surface (Schmocker and Hager, 2009). In contrast, using a side view does not apply for monitoring fluvial dike breaching, because the breach evolution is asymmetric. Readers are referred to Bouratsis *et al.* (2013), Massot-Campos and Oliver-Codina (2015), Chourasiya *et al.* (2017) and Friedl *et al.* (2018) for extensive reviews of underwater measurement techniques for evolving beds. Hereafter, three key applications of imagery based, non-intrusive systems for monitoring dam or dike breaching through the water surface are reviewed and compared.

Pickert *et al.* (2004, 2011) conducted experiments on embankment dam breaching induced by flow overtopping. The evolving geometry was monitored by the Fringe Projection technique, which consists in projecting parallel fringes on the dam by a video projector. The incidence of fringes on the dam geometry was recorded by a high speed camera through the flume glass sidewall. This non-intrusive technique required, however, painstaking calibration for each fringe that has to be adjusted for glass/air and glass/water interfaces. A significant manual correction procedure was applied to reduce inaccuracies due to refraction effects. The Fringe Projection technique provides accurate reconstruction of the embankment geometry during the first breaching phases, but fails to reconstruct large breaches because of the high water turbidity reducing significantly the visibility of fringes (Schmocker, 2011). The complexity of the technique increases further when the water surface is rough and wavy (Chourasiya *et al.*, 2017). A major advantage of the technique lies in its ability to reconstruct even overhanging blocs, promoting therefore the use of the method for cohesive dike breaching experiments.

Frank and Hager (2014, 2015) captured the basic topographical embankment dam breach features by a 3D photogrammetry measuring system, using the commercial stereoscopic-videometric system AICON (Henning *et al.*, 2008). Four synchronized CCD cameras recorded a 25 mm spacing grid projected over the dike. Three cameras were used for the dam geometry reconstruction, while the fourth one recorded the water surface level through the flume side glass wall. The experimental setup was darkened to obtain a sharp grid contrast on the dam surface. The refraction correction was performed assuming a horizontal water level across the entire channel width. One crucial requirement of photogrammetry is the recognition of a same marker on multiple frames (i.e., homologous points), which can be particularly laborious in homogeneous surfaces, such as sand dikes. The AICON 3D system overcomes this issue by performing the cross-identification on the grid nodes. The resolution of the final reconstruction was, at most, equal to the grid spacing, i.e., 25 mm.

Spinewine *et al.*'s (2004) dam breaching experiments were monitored using the Laser Profilometry Technique (LPT). The dam was continuously swept with a laser sheet reflected on a tilting mirror; one complete sweeping lasted about 5 s, which was considered as quasi-instantaneous with respect to the breach evolution rate (Spinewine *et al.*, 2004). The recording was performed by a high speed camera and images were then processed to extract laser profiles (Capart *et al.*, 2002; Spinewine *et al.*, 2004). No distinction was made between the submerged and emerged parts of the dam in the reconstruction processes. Precision and resolution of the final reconstruction depended, among others, on the laser sweeping speed, the shutter speed, the recording frame rate, and the frame resolution. Errors on the dam surface elevation due to refraction were estimated to be of the order of 30 mm.

Chourasiya *et al.* (2017) and Wallner (2014) used the commercial Microsoft Kinect® 3D depth sensor to monitor the breach evolution. This device, as other RGB-D (i.e., RGB image and Depth) sensors, combines an infrared projector, an infrared camera, and a digital camera. The infrared sensor projects a speckle pattern that is reflected on the target geometry. The deformed pattern is captured by the infrared camera and is correlated against a reference speckle pattern projected on the surface at known distance from the sensor to construct a 3D map of the object. Reconstructed geometries by Wallner (2014) showed missing spots as the Kinect sensor was highly sensitive to lighting conditions and visibility. Chourasiya *et al.* (2017) outlined the range of applicability of the Kinect in terms of model dimensions and water turbidity, and proposed a refractive correction for measurements recorded in presence of water. However, the resolution of the infrared sensor was relatively low (640 × 480 pixels), limiting therefore the use of the technique for monitoring larger scale mobile bed models.

Overall, the aforementioned techniques are relatively comparable, as they rely on image processing. In subaqueous conditions they remain, however, affected by three major issues:

(i) visibility, which is influenced by the lighting conditions, projection power, water turbidity, as well as by the model scale;

(ii) refraction, which bias can be addressed if the water depths are accurately measured within the domain under moving bed conditions without altering the physical processes (the extent and direction of refraction bias can therefore be roughly estimated in advance and included in the interpretation of the results);

(iii) and reflections, which (unlike refraction) cause absence of data and therefore a scattered description of the bed surface at the underneath areas.

Compared to other methods (e.g., fringes or grid projection), reflections are less of a concern for LPT, because in the LPT only a single laser profile needs to be identified in each image. Should parts of the projected laser sheet be reflected on the water surface, these reflections appear as outliers and are straightforward to filter out automatically, without any interference with other parts of the laser profile. In contrast, in the case of a projected mesh, reflections of some parts of the projected pattern on the water surface are likely to interfere with other parts of the projected pattern, leading to larger patches impossible to process.

Table 1 assesses and compares the applicability of the aforementioned techniques for fluvial dike breaching experiments. It should be noted that experiments of Frank and Hager (2014) and Pickert *et al.* (2004, 2011) relied partially or totally on video recordings through the transparent sidewall of the flume. This is not feasible in a fluvial configuration, because the assumption of symmetrical dike breach evolution is no longer relevant (Rifai *et al.*, 2017). In light of each technique advantages and shortcomings, and in regards of cost and implementation efforts, the LPT was selected for the present work to capture the continuously deforming dike surface. This method and variants were applied in similar studies, including morphological changes induced by dam-break wave over mobile channel beds (Soares-Frazão *et al.*, 2007), bed scouring due to planar turbulent wall jet (Younkin and Hill, 2009), bed scouring around hydraulic structures (Tian *et al.*, 2010), debris flows (Hung and Capart, 2013), and submerged migrating sand waves (Hoshino and Yasuda, 2015).

Table 1. Evaluation of selected non-intrusive techniques used for continuous monitoring of dike breaches

Method	References	Rapidity	Data density	Refraction correction	Vertical accuracy
Fringe projection	Pickert *et al.* (2004, 2011)	7.5 frames/s	Fringes of 7 mm in width	Manual corrections	Good accuracy, but significant manual corrections
Laser profilometry	Spinewine *et al.* (2004)	One sweeping cycle: 5 s	High density	None	Of the order of 30 mm due to refraction effects
Kinect sensor	Wallner (2014)	30 frames/s	Relatively low (due to infrared sensor resolution)	None	Poor due to refraction effects
	Chourasiya et al. (2017)			Correction equation	Of the order of 5 mm
Photogrammetry	Frank and Hager (2014, 2015), Frank (2016)	Up to 30 frames/s	25 mm grid spacing	Automated correction accounting for water level measurements	2 mm, except in zones with high transverse slope of water surface (up to 10 mm)

3 METHODOLOGY AND IMPLEMENTATION

The LPT relies on the sweeping of a laser sheet on the geometry of interest, i.e., the dike in the present work. The sweeping of the illuminated laser line incident on the geometry is recorded by a digital camera. Image processing allows segregation of the deformed laser lines referenced in the 2D image coordinates. Prior calibration of the camera, along with referencing of the projected laser profiles, allow the reconstruction of the laser profiles on the 3D object coordinates. Each frame allows the reconstruction of a single laser profile. Submerged parts of the laser profiles are identified and processed within the refraction correction module. The reconstructed profiles of a full one way laser sweeping are combined to construct a point cloud representing the bed at each instant.

In the following, we describe the laboratory setups on which the LPT was developed, we introduce the algorithm used for calibrating the camera, and we detail the image processing to generate the dike topography reconstructions.

3.1 Laboratory experimental Setups

Physical modeling to support this research was described in detail by Rifai *et al.* (2016, 2017, 2018, 2020) and the dataset has been made available (Rifai *et al.*, 2019b). Two experimental setups were built, both equipped with the LPT system: the ULiège model in the Engineering Hydraulics Laboratory of the University of Liège, Belgium, and the EDF model in the experimental facilities of the National Laboratory for Hydraulics and Environment (LNHE) of EDF R&D, France. In both models, the dike material was uniform coarse sand of a median diameter of 1 mm.

For the ULiège model, a Z-Laser Z30M18S3-F-640-LP75 with a 75° fan angle and a 30 mW power was used. The recording was performed with a Panasonic GH4 camera set to Full-HD resolution, i.e., 1920 × 1080 pixels with a frame rate of 60 frames/s. For the large scale EDF model, two LAP-UD 30 mW lasers were minutely aligned to have coplanar projected sheets, and a Canon EOS 6D Mark II camera was used with the same recording resolution and frame rate as those of the ULiège model. However, the sweeping motion was not the same (Figure 2): in the ULiège model, the laser was tilting around a horizontal axis, whereas in the EDF model the laser was translated along a horizontal rail because a tilting motion was deemed not adequate to guarantee the required precision. In both models, one complete dike sweeping lasted between 1.5 s and 5 s. It enabled harvesting about 90 laser profiles. The lighting of the laboratory facilities was adjusted in order to minimize light reflections.

Selected experiments are presented in this paper, but the focus is on the demonstration of the capabilities of the LPT, rather than on the findings of the fluvial dike breaching experiments. Readers may refer to the works carried out by Rifai *et al.* (2017, 2018) for more details.

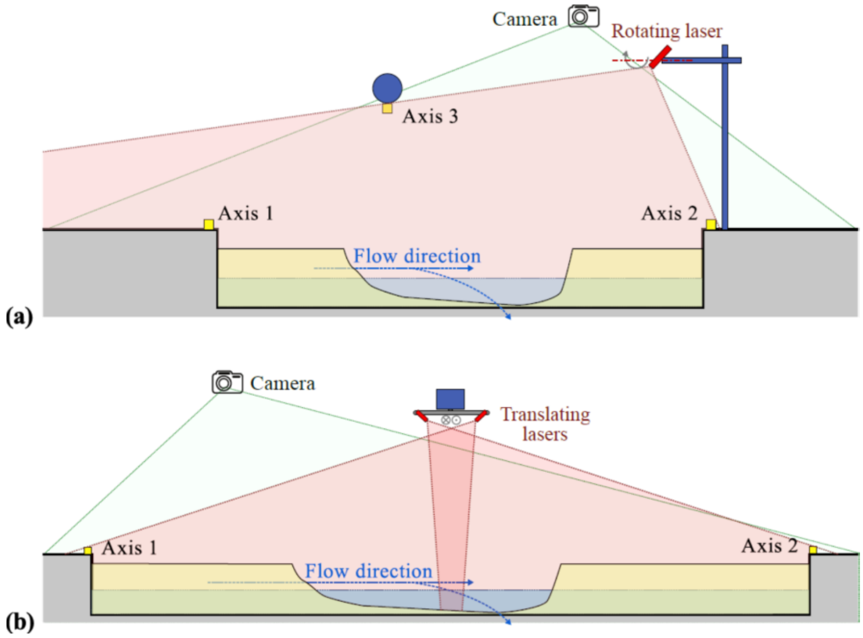

Figure 2. Layout of the laser in (a) ULiège setup, and (b) EDF setup. Axes 1 to 3 are the reference axes used for determining, for each image, the equation of the plane of the projected laser sheet (see Section 3.4).

3.2 Calibration of the camera

The calibration of the camera consists in building the system of equations transforming the image coordinates of each point on the camera sensor to a viewing ray defined in the world referential. Here, the Direct Linear Transformation (DLT) (Abdel-Aziz and Karara, 2015) is used to calibrate the camera, as detailed in Supplemental Material (Text S1). The algorithm accounts for optical and decentering image distortion.

In the DLT algorithm, the camera calibration is performed through the computation of sixteen parameters (noted L_i) by solving a nonlinear system expressing the transformation of coordinates for a set of n "control points" (Abdel-Aziz and Karara, 1971; Morasso and Mohan, 2006). Control points are physical points whose object coordinates (x, y and z) have been measured in the laboratory and the corresponding image coordinates (u, v) have been determined manually. They are used for identifying the DLT parameters (L_1 to L_{16}).

In general, at least eight non-coplanar control points are needed. In the present work, more than twenty control points are used. Moreover, different weights are assigned to the individual control points, depending on the variance of the random error components, which are calculated considering the variance of the image plane coordinates and object coordinates of the control points to a random noise. High variance points have smaller weights. Details of the method are given by Marzan and Karara (1975).

The control points must be distributed as uniformly as possible in both the object coordinate system and in the image coordinate system. Processing points located outside the volume and/or surface covered by the control points should be avoided. Coplanarity of the control points should also be avoided, because it deteriorates the condition number of the system to be solved for obtaining parameters L_1 to L_{16}.

3.3 Identification of the laser profiles

For each image i, identifying the laser profile $I_i(u)$ in the image coordinates involves three steps. The first one consists in selecting, for each pixel (u, v) of each of the three RGB (Red, Green, and Blue) layers, the median value over a set of images. It gives a background image, which in the second step is subtracted from each processed image. This procedure is efficient in reducing noise and leads to a better segregation of the laser profile. Finally, a red chrominance filter is applied on each image. Further details are given in Text S2 in Supplemental Material.

Figure 3 illustrates how the conversion of the raw image to a red chrominance layer allows an efficient segregation of the laser profile. The laser profile is then defined as the vector composed, for each u, of the v coordinate of the maximum red chrominance pixel. This method for constructing the laser profile vector I_i does not allow defining multiple points along the same u coordinate. This issue is overlooked in the present work, given the scope of the dike breach experiments, the selected view point of the camera and the angle of laser sweeping.

The LPT requires neither the camera intrinsic parameters nor the definition of positions and orientations of the camera and laser (except on the EDF model where the laser plane at the initial position is determined by *in-situ* measurements). There is therefore a flexibility in the setup of the camera and laser emission device which can be moved between the tests as the calibration steps require only the control points and laser reference axes.

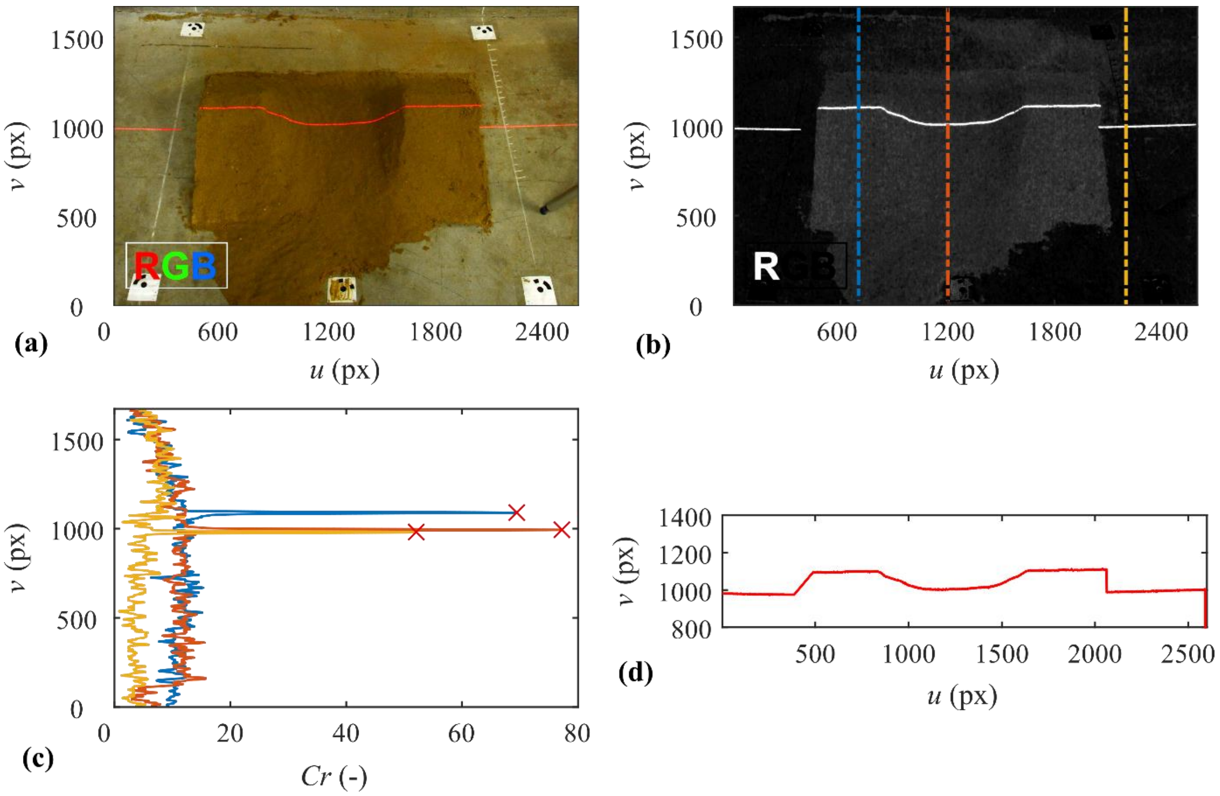

Figure 3. Illustration of image filtering steps: (a) raw image, (b) red chrominance component of the image, (c) red chrominance *Cr* at three different *u* (see (b)), and (d) resulting laser profile. In Fig. 3a, four white squares with embedded black dots are targets (not used in the present study).

3.4 Laser plane reconstruction

The principle of the LPT is based on the fact that the location of each point of the laser profile is the intersection between the viewing ray and the plane corresponding to the projected laser sheet. Therefore, the identification of the laser plane in each frame is necessary for constructing the transformation matrix allowing the conversion of each point in the image frame to its corresponding object point.

The identification of the laser plane, in the object coordinate, consists in determining the equation of this plane by locating the intersection of the laser plane with at least three non-coplanar axes (Figure 4). These axes are previously referenced in the object and image coordinate systems. The mathematical formulation used for determining the plane equation is presented in Text S3 in Supplemental Material.

For the ULiège model, three horizontal reference axes are set which allow for a direct evaluation of the laser plane equation parameters for each frame (Figure 2a). The EDF model has only two reference axes (Figure 2b), because of the model scale, laser fan angle, and camera view point. In EDF model, the projected laser sheets are translated along a rail parallel to the reference axes. The inclination angle of the laser sheet is calculated on site *prior to* tests, and therefore two points are sufficient to compute the laser plane in each frame *i* because all the laser planes are parallel.

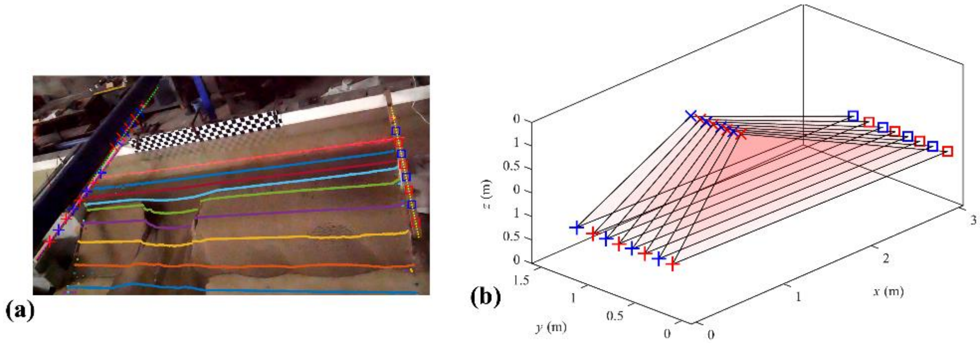

Figure 4. Example of localisation of intersection of laser plane and laser reference axes on the ULiège model in (a) recording frames, and (b) reconstructed in object coordinate system.

3.5 Point cloud reconstruction

The point reconstruction step consists in converting image points of the laser profile into the object coordinate system. This is achieved by solving, for each point, a three-equation linear system, whose unknown variables are the object coordinates of the considered point (see Text S4 in Supplemental Material). The first two equations of the system correspond to the equations of the viewing ray linking the considered point to its projection in the image plane. The third equation is the laser plane equation in the corresponding frame. Solving the linear system is equivalent to finding the intersection between the view ray and the laser sheet.

3.6 Refraction correction

Once each point of the laser profile is reconstructed in the object coordinate system, each point is checked whether it is submerged or not. This step is based on the comparison of the location of the point on the image frame and submerged contours, manually defined by visual inspection, for each sweeping (Figure 5).

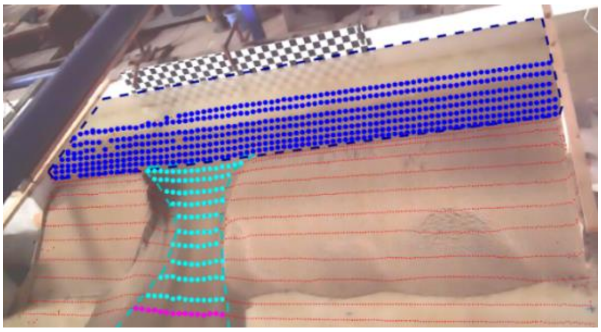

Figure 5. Example of submerged zone contours, (·) laser profiles, (●) main channel, (●) breach, and (●) floodplain.

If a point lies outside the contours, its coordinates are added to the point cloud. Otherwise, a refraction correction is applied. This correction requires multiple steps (detailed in Text S5 in Supplemental Material):

(i) the refraction correction requires a detailed knowledge of the water surface, in particular, locally, the water surface elevation and the vector normal to the water surface. In this work, water levels are measured pointwise and a detailed description of the water surface is not directly available. Instead, a synthetic water surface is constructed based on the water level measurements in the main channel. Three areas are defined (Figure 6a): (i) channel (C), (ii) breach (B), and (iii) floodplain (F). The channel surface C consists of a horizontal plane whose elevation equals the mean measured water elevation in the main channel. The breach surface B is an inclined plane starting from the intersection between the surface C and the upstream face of the dike (point E_{CB}) to a specified point (E_{BF}) at the dike downstream toe. The floodplain surface F is a horizontal plane at a prescribed elevation. This gross description induces residual errors in the refraction corrected points. Figure 6b illustrates the induced errors. For instance, when the water surface is actually higher than the synthetic water surface, the final reconstruction is slightly higher than the real state of the dike;

(ii) for various points of the laser profile, the intersection of the projected laser sheet and the synthetic water surface (C, B or F) is determined; and the direction of the refracted laser sheet is determined by Snell-Descartes law (Glassner, 1989);

(iii) the view ray computed with the DLT parameters of a submerged point is in reality the line connecting the point P_B to the camera principal point (Figure 6a). From this biased view ray, and knowing the water surface W, the intersection point P_B is determined. Then, knowing the directing vector from P_B toward the camera, and the vector normal to W, the non-refracted view ray can be deduced;

(iv) and finally, the point P_C is the intersection of the refracted laser plane and the non-refracted view ray (Figure 6a).

The main assumption underlying the refraction correction presented here is the idealised shape of the considered synthetic water surface, which follows an inclined plane in the breach and horizontal planes in the main channel and floodplain. A more elaborate approach was introduced by Frank and Hager (2014, 2015) and Frank (2016), who used the actual water surface as determined by means of a side camera. This approach is, however, not directly applicable in the present work due to the asymmetric breach development that prevents the use of a side camera.

(a)

(b)

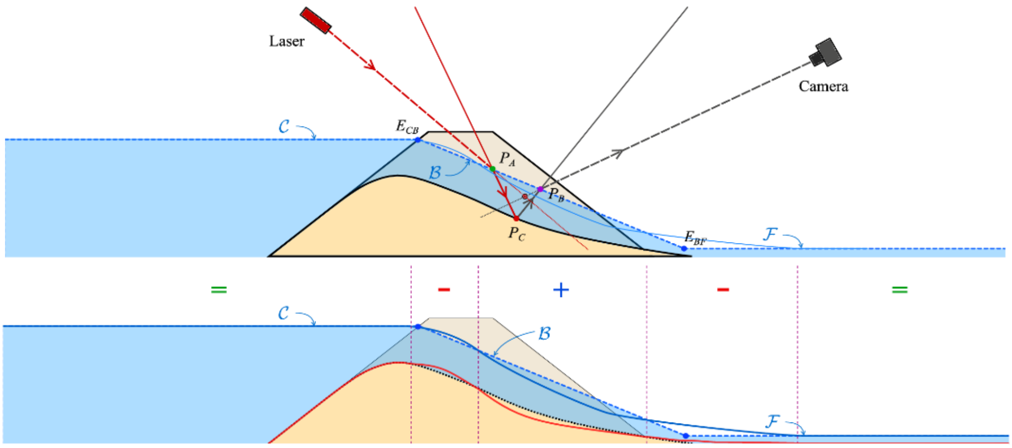

Figure 6. (a) Illustration of water refraction effect on projected laser sheet and view rays and (b) residual refraction bias (not to scale).

4 RESULTS AND ACCURACY ASSESSMENT

As preliminary tests, the LPT was applied for a dry wooden trapezoidal dike of known geometry, to demonstrate the measurement repeatability when the camera position, view angle and laser position were varied (see Text S.6 in Supplemental Material). Then tests on simple configurations under dry and subaqueous conditions were performed. Finally, the LPT was used for monitoring fluvial dike breaching experiments conducted on two distinct laboratory models. The following tests are presented hereafter:

(i) comparison between the LPT reconstruction and the results obtained with a laser scanner Focus-3D (designed by FARO®), in dry conditions;

(ii) tests with known rigid dike geometries (idealized dike and partially breached dike), to assess the refraction correction, and the 3D reconstructions in submerged conditions;

(iii) and two case studies of evolving fluvial dike breaching experiments, i.e., ULiège model and EDF model, with the assessment of deviations in the 3D reconstructions.

4.1 LPT versus laser scanner Focus-3D in dry conditions

The LPT was compared to the laser scanner Focus-3D which can be applied only under dry conditions (Die Moran *et al.*, 2013; Claude *et al.*, 2018). The initial and the final dike geometry, after flow overtopping and breach expansion, were measured by both techniques (Figure 7). The laser scanning was performed by placing the laser scanner at two locations and then combining the resulting point clouds, allowing a complete coverage of the dike. Note that the measurement duration with the laser scanner Focus-3D is long, e.g. obtaining the results shown in Figure 7 required a 30 min scan. Differences between the two geometry reconstructions were relatively low, with a median absolute error of 9.5 mm and 95 % of the reconstructed areas points having an error below 16 mm.

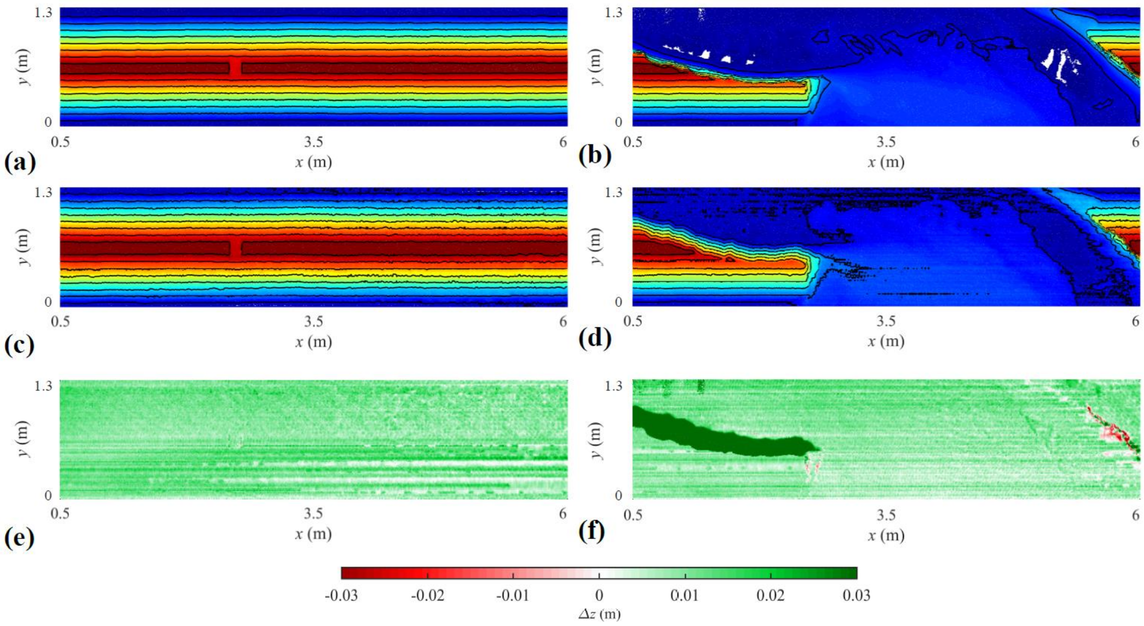

Figure 7. Comparison of 3D reconstructions: (a) Focus-3D scan of initial dike, (b) Focus-3D scan of final dike, (c) LPT reconstruction of initial dike, (d) LPT reconstruction of final dike, (e) difference between (a) and (c), and (f) difference between (b) and (d).

4.2 Refraction correction

To assess the refraction correction, we performed two types of tests. First, we considered an idealized trapezoidal wooden dike of known geometry, 75 cm long, 87 cm wide, and 20 cm high, with a side slope of 1V:2H and a 0.07 m wide crest (Figure 8a). The water level was set 6 cm above the dike crest. Figures 8b and d illustrate the results obtained without applying the refraction correction. Compared to the reference geometry, the reconstruction is inaccurate, as the obtained dike is up to 10 cm higher than the real geometry. Overall, the trapezoidal shape of the dike-like geometry was tilted and flattened in this reconstruction. Accounting for the refraction correction considerably improved the accuracy of the results (Figures 8c and d). The remaining irregularities on the upstream dike slope may be attributed to the water surface rippling and to reflection on the water surface (Figure 8a). In this example, the refraction correction module allows reducing the reconstruction errors from 20 mm to 10 mm on the dike crest (areas with 6 cm of water depth) and from 80 mm to 10 mm on lower sides of the dike slope (areas with 26 cm of water depth).

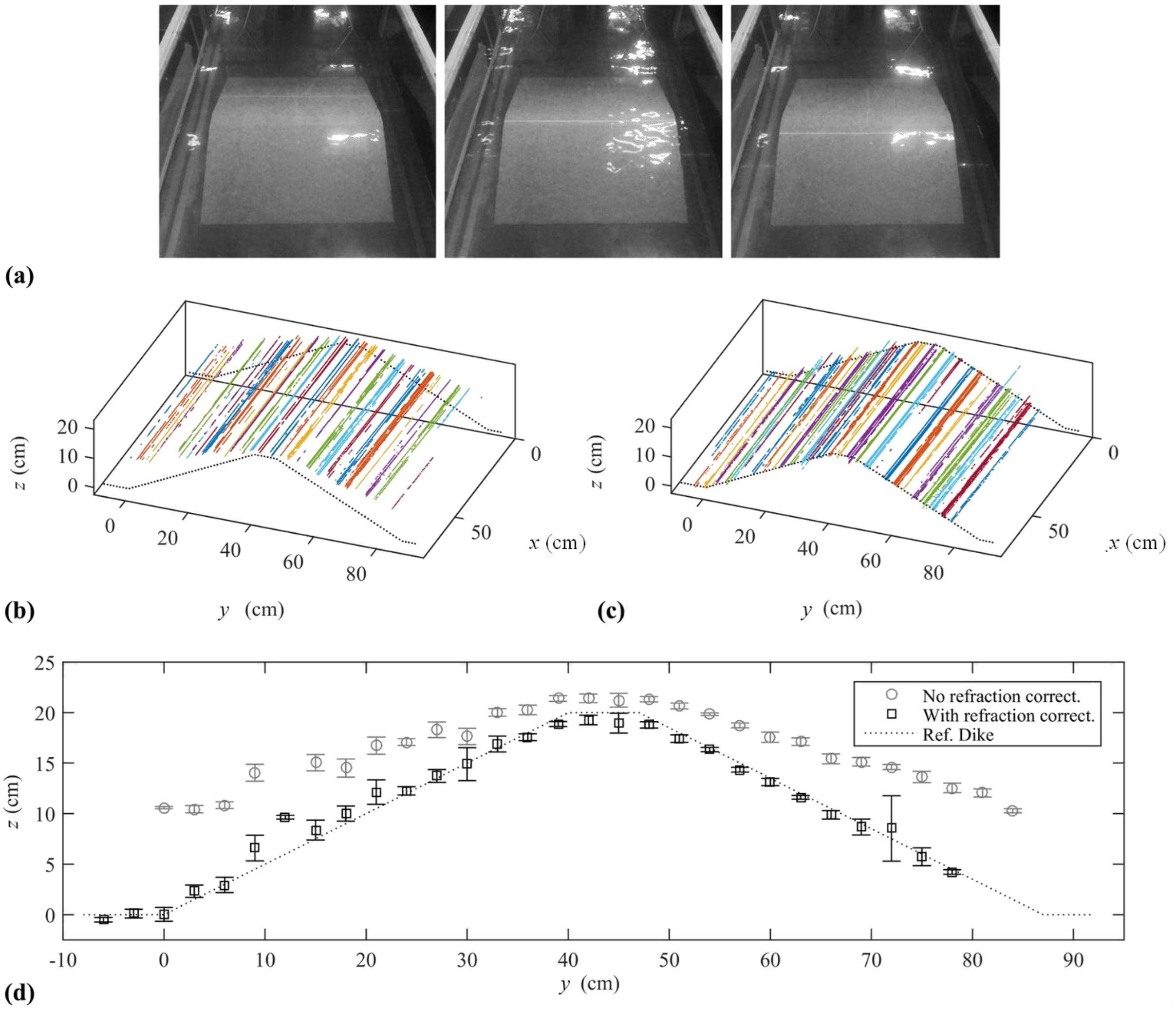

Figure 8. 3D reconstructions of the submerged wooden dike: (a) camera view of the laser sweeping on the dike, (b) 3D reconstruction without refraction correction, (c) 3D reconstruction after refraction correction, and (d) side longitudinal view of reconstructions compared to the reference exact dike geometry.

To assess the validity of the refraction correction in a more general setting (involving the assumption of a synthetic prismatic water surface, as detailed in Section 3.6), a series of tests was conducted on the ULiège model using a plastered irregular breached dike. To generate reference data, the geometry of the dike was measured accurately in dry conditions using a laser distancemeter mounted on an automatic traverse system. Results highlight a substantial improvement of the agreement between the LPT results and the reference data when the refraction correction is activated (Figure 9). However, the effect of refraction is overestimated at some specific locations (e.g., at x = 1.2 m). The errors between the submerged and non-submerged reconstructions were typically around 60mm and 30 mm, at the channel area and breach area, respectively. The errors dropped to around 30 mm and 18 mm, respectively, after the refraction correction was performed.

Overall, the residual bias after refraction correction, resulting from measurement inaccuracies and the simplified representation of the water surface, relates generally to the submerged length of the laser sheet and view rays, and hence to the water depth, the free surface inclination and the camera positioning.

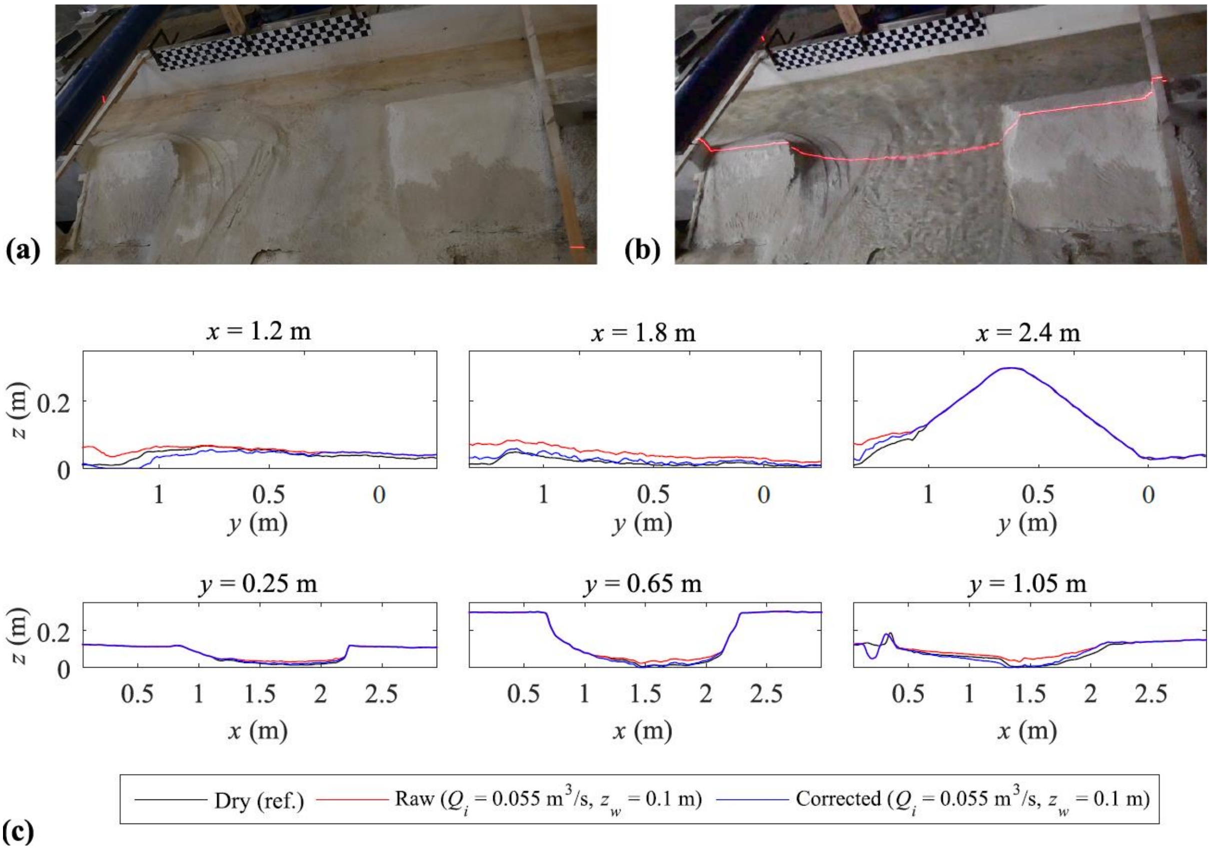

Figure 9. Tests of refraction correction module on the ULiège model: (a) non-submerged plastered dike, (b) submerged plastered dike, and (c) comparison of cross sectional and longitudinal reconstructions. The main channel flow discharge Q_i = 0.055 m^3/s and the initial water level in the main channel z_w = 0.1 m.

4.3 Accuracy assessment

Several sources of errors in the final reconstruction may be spotted in the LPT procedure. Hereafter, we discuss sources of discrepancy regarding: (i) the manual determination of the control points on the image coordinates (error represented by the random variable v_i), (ii) *in-situ* measurement of the position of the control points in the object coordinates (random variable v_{ii}), (iii) location of the laser profile in the images (random variable v_{iii}), (iv) location of the intersection of the laser plane with the laser reference axes (random variable v_{iv}), and (v) water level estimation (random variable v_v).

Errors in the final reconstructions were evaluated by propagating through the reconstruction procedure the probability density functions (PDF) of the errors in the inputs. A normal distribution was assumed for the random variables v_i, v_{ii}, and v_{iii} because the determination of these variables is aimed toward a real-value with a random noise. A uniform distribution is associated to the variables v_{iv} and v_v. For each of these variables, which are taken separately, 60 samples were tested and 600 samples were tested with all combined variables.

Figure 10 illustrates the accuracy of the final 3D reconstructions in partially submerged (i.e., during the breach expansion) and in dry conditions (i.e., end of the experiment) for ULiège model. In the partially submerged case, the highest deviations are located in the upstream part of the breach and in the submerged channel face of the dike. On the left side of the dike (x < 1.5 m), which is the most remote from the camera, the vertical deviations reach 10 mm in non-submerged areas and 20 mm in submerged areas. In the floodplain-side face of the dike (y > 0.8 m), the standard deviation of the vertical deviations reaches 20 mm due to the quasi co-planarity between the laser sheet and the dike face. Cross sections of Figure 10 are presented Text S7 in Supplemental Material.

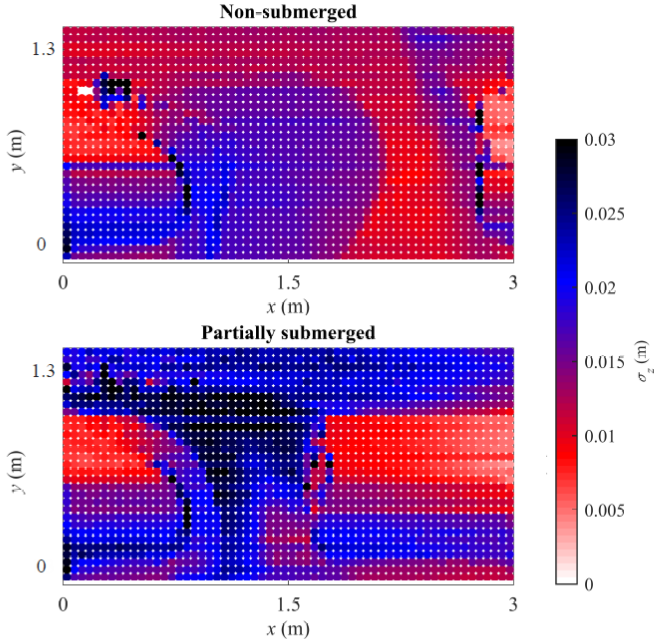

Figure 10. Deviations in the final 3D LPT reconstructions of the ULiège model, with σ_z the standard deviation of the reconstructed elevations *z* of the dike.

Investigating discrepancy related to each of the sources individually shows that reconstruction is highly sensitive to the determination of the control points in the object coordinate system. This step is performed only once and, therefore, the same control point object system referencing is used for all the reconstructions.

In the ULiège model, the camera is located at $x \approx 2.5$ m, $y \approx -3.54$ m, and $z \approx 2.5$ m. This is consistent with the lower precision due to other input variables, in particular, the laser profile construction (v_{iii}) and localisation of the intersection of the laser plane with the laser reference axes (v_{iv}), as the further the object is from the camera, the larger portion of the object is represented by just a single pixel.

For the EDF model, the sweeping was recorded with the same resolution and speed as for the ULiège model. The same PDFs and sampling method were also used. The camera was located at $x \approx 1$ m, $y \approx -4$ m, and $z \approx 3.5$ m. Similarly to the ULiège model, the main deviations in geometry reconstruction are due to control point referencing in the object coordinates. Under submerged conditions, the lowest accuracy is obtained in the submerged parts of the dike breach. For the non-submerged case, the highest accuracy is obtained further downstream from the camera location ($x > 4$ m). The center part of the main channel seems to be less accurately reconstructed in the submerged case, which can be due to a sensitivity of the distortion correction and/or an inadequate distribution of the control points used for the calculation of the DLT parameters. Moderate deviations are spotted on the floodplain face of the dike, probably because the laser sheet is translated in the case of the EDF model (same inclination of the laser plane during the sweeping) and the laser plane is more coplanar with the floodplain-side face of the dike and more perpendicular to the channel-side face.

Overall, errors in the EDF setup are reduced by a factor of two in comparison with the ULiège setup (maximum deviations of 15 mm instead of 30 mm). This improvement can be explained by the replacement of the rotating laser used in the ULiège model by a translating one in the EDF model. This change slightly compromised the flexibility of the method because the laser needs to be precisely calibrated if it is moved. However, the reconstruction of the laser sheets was more stable because the used intersection points were more in the vicinity of the volume defined by the control points. In addition, more control points (≈ 40) were used in the EDF model, thereby contributing to the robustness of the reconstruction with respect to errors in the identification of the control points. Cross sections of Figure 11 are presented Text S7 in Supplemental Material.

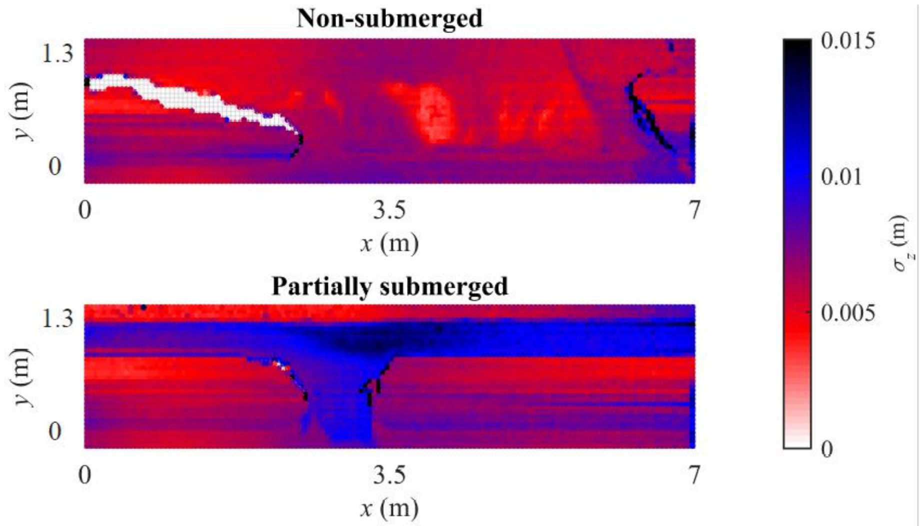

Figure 11. Deviations in the final 3D reconstructions of dike breach in the EDF model, with σ_z the standard deviation of the reconstructed elevations z of the dike.

4.4 Comparison with other methods

Among the different studies introduced in Section 2 (Table 1), only Frank and Hager (2014, 2015) and Frank (2016) provide a systematic and quantitative assessment of the performance of their method. We compare here the accuracies obtained with the LPT with those of the photogrammetry technique set up by Frank and Hager (2014, 2015) and Frank (2016).

For various experimental settings, Table 2 reports the accuracy of the LPT and the photogrammetry technique. The maximum deviations, between 10 mm and 20 mm, are generally comparable between the two methods. Nonetheless, in non-problematic areas the photogrammetry seems to reach a slightly higher accuracy than the LPT (± 2 mm *vs*. ± 5 mm). However, for high flow discharges, the photogrammetry leads to relatively large patches where grid points are not recognized by the system (Frank, 2016). This is less of a concern for the LPT.

Compared to the duration of one sweep of the LPT (about 5 s), the photogrammetric system captures the data instantaneously, with a frequency up to 30 Hz. This can be an advantage at during the rapid breach erosion phase at the start of breaching.

Table 2. Accuracy of the LPT compared to Frank and Hager (2014, 2015) and Frank's (2016) photogrammetry technique.

Experimental settings	Photogrammetry	LPT
Comparison with laser scanner Focus-3D in dry conditions: initial and breached dikes (EDF model)		Vertical deviation generally below 10 mm and, at maximum of the order of 30 mm in blind sports not covered by LPT
Immerged objects of known geometry (submergence of 6 to 8 cm)	Cube: absolute deviations of ± 2 mm for plane surfaces; but poor accuracy at the corners (due to 25 mm grid spacing)	Trapezoidal wooden dike: deviations remain mostly below 2 mm
Fixed spatial dike breach	Deviations mostly below 2 mm, and maximum deviations of 10 to 20 mm in zones of steep water or sediment surfaces	Mostly below 5 mm, and maximum deviations of 10 to 20 mm in areas most remote from the camera, or quasi with the laser sheet
Error propagation (ULiège model)		Mostly below 10 mm, maximum 30 mm
Error propagation (EDF model)		Mostly below 5 mm, maximum 15 mm

5 CONCLUSION

A non-intrusive, high resolution Laser Profilometry Technique (LPT) developed specifically for uninterrupted monitoring of 3D evolving breach geometries in laboratory experiments of fluvial dikes has been presented. It has been implemented on two laboratory setups, one at the University of Liège (ULiège model) and the second one at EDF R&D (EDF model).

On the EDF model, the LPT was compared to the laser scanner Focus-3D which applies only under dry conditions. The discrepancies for this case remained mostly below 10 mm, except in blind spots not covered by the LPT, where data were interpolated. The performance of the refraction correction for submerged conditions was emphasized based on two series of tests carried out on the ULiège model, in which the LPT results were compared to a dike-like known geometry and to independent measurements of a partly breached dike. The differences between the LPT reconstructions and the actual geometry were mostly below 5 mm on average, and they did not exceed 10 to 20 mm locally (in the most remote areas from the camera, and on surfaces nearly coplanar to the laser sheet).

Accuracy of the final 3D reconstructions was evaluated by means of error propagation through the LPT algorithm. For submerged conditions, the lowest accuracy was found in the upstream part of the breach and on the channel-side face of the dike. The analysis revealed that the reconstruction is highly sensitive to the determination of the control points. Increasing the number of control points strongly increased the accuracy. Moreover, the deviations are reduced by about a factor two when the laser sheet is translated instead of being rotated (maximum deviations of 15 mm instead of 30 mm).

The LPT leads to an accuracy (~ 5 mm) relatively comparable to that of other state-of-the-art techniques for continuous monitoring of submerged bed evolution, such as the photogrammetry method developed by Frank and Hager (2014, 2015) and Frank (2016) whose accuracy can reach about 2 mm in non-problematic zones. Moreover, the LPT offers additional advantages. Indeed, compared to more standard non-intrusive distributed methods (i.e., fringe projection or close-range photogrammetry), the LPT is less sensitive to artefacts resulting from reflection on the water surface, particularly in the vicinity of the breach where the free surface is irregular and wavy. The LPT is relatively low-cost as it is based on the use of a commercial digital video camera and a sweeping red diode laser projecting a sheet over the fluvial dike. Neither the position of the camera, its orientation and intrinsic characteristics nor the laser position have to be determined prior to measurements. The information needed for the reconstruction process are encapsulated in the recording, conferring to the method a high flexibility.

In line with Frank (2016), a promising strategy for improving the refraction correction algorithm consists in measuring the water levels in a separate model run and subsequently applying this measured water level distribution when correcting for refraction in a repetition of the test. This requires careful verification of repeatability of tests. Besides, further adjustments are needed for the application of the LPT to cohesive dike breaching due to the reduced visibility resulting from the higher turbidity of water.

ACKNOWLEDGEMENTS

The authors acknowledge the support of the *Fonds Spéciaux de la Recherche* (FSR) of the University of Liège, Belgium. The work was partially funded by the *Association Nationale de Recherche et de la Technologie* (ANRT) [CIFRE #2015/0015], the European Fund FEDER (*Programme Opérationnel Interrégional Rhône-Saône* 2014-2020) and EDF.

The dataset obtained from the laboratory experiments has been made available: https://doi.org/10.5281/zenodo.1494800.

The AE and two anonymous reviewers are gratefully acknowledged for their valuable comments and suggestions.

AUTHOR CONTRIBUTIONS

I.R., S.E., B.D., P.A., M.P. and K.E.A. contributed to the design of the model of ULiège and to the development and implementation of the LPT. I.R., K.E.A. and D.V. contributed to the design of the model of EDF R&D, and the adaptation of the LPT. I.R. conducted all experiments and processed all data. S.E., B.D., P.A. and M.P. provided support for conducting the tests at ULiège and processing the corresponding data. K.E.A. and D.V. provided support for conducting the tests at EDF R&D and, together with B.D., they helped in the processing of the corresponding data. I.R. wrote the first draft of the paper. I.R., B.D., V.S. and K.E.A. revised successive versions of the paper.

REFERENCES

Abdel-Aziz, I. Y, & Karara M. H. (2015). Direct linear transformation from comparator coordinates into object space coordinates in close range Photogrammetry. Photogrammetric Engineering and Remote Sensing 81(2): 103-107. doi: 10.14358/PERS.81.2.103.

Amaral, S., Caldeira, L., Viseu, T., & Ferreira. R. M. L. (2020). Designing Experiments to Study Dam Breach Hydraulic Phenomena. Journal of Hydraulic Engineering 146(4): 04020014. doi:10.1061/(ASCE)HY.1943-7900.0001678.

Bailly, J. S., Le Coarer, Y., Languille, P., Stigermark, C. J., & Allouis, T. (2010). Geostatistical estimations of bathymetric LiDAR errors on rivers. Earth Surface Processes and Landforms 35(10): 1199-1210. doi: 10.1002/esp.1991.

Bouratsis, P., Diplas, P., Dancey, C. L., & Apsilidis, N. (2013). High resolution 3-D monitoring of evolving sediment beds. Water Resources Research 49(2): 977-992. doi: 10.1002/wrcr.20110.

Brasington, J., Vericat, D., & Rychkov, I. (2012). Modeling river bed morphology, roughness, and surface sedimentology using high resolution terrestrial laser scanning. Water Resources Research 48(11): W11519. doi: 10.1029/2012WR012223.

Capart, H., Young, D. L., & Zech, Y. (2002). Voronoi imaging methods for the measurement of granular flows. Experiments in Fluids 32(1): 121-135. doi: 10.1007/s003480100351.

Challis, J. H., & Kerwin, D. G. (1992). Accuracy assessment and control point configuration when using the DLT for photogrammetry. Journal of Biomechanics 25(9): 1053-1058. doi: 10.1016/0021-9290(92)90040-8.

Chourasiya, S., Mohapatra, P. K., & Tripathi, S. (2017). Non-intrusive underwater measurement of mobile bottom surface. Advances in Water Resources 104: 76-88. doi: 10.1016/j.advwatres.2017.03.009.

Claude, N., Leroux, C., Duclercq, M., Tassi, P., & El kadi Abderrezzak, K. (2018). Limiting the development of riparian vegetation in the Isère River: a physical modelling study. Proc. 9th International Conference on Fluvial Hydraulics (River Flow), Lyon. doi: 10.1051/e3sconf/20184002015.

Dazzi, S., Vacondio, R., & Mignosa, P. (2019). Integration of a levee breach erosion model in a GPU-accelerated 2D shallow water equations Code. Water Resources Research 55(1): 682-702. doi: 10.1029/2018WR023826.

Dewals, B., Rifai, I., El kadi Abderrezzak, K., Greco, M., Di Cristo, C., Iervolino, M., Leopardi, A., & Vacca, A. (2018). Numerical simulation of lateral dike breaching due to overtopping. Proc. 9th International Conference on Fluvial Hydraulics (River Flow), Lyon. doi: 10.1051/e3sconf/20184003025.

Die Moran, A., El kadi Abderrezzak, K., Mosselman, E., Habersack, H., Lebert, F., & Aelbrecht, D. (2013). Physical model experiments for sediment supply to the Old Rhine through induced bank erosion. International Journal of Sediment Research, 28(4): 431-447. doi: 10.1016/S1001-6279(14)60003-2.

Elalfy, E., Tabrizi, A. A, & Chaudhry, M. H. (2017). Numerical and experimental modeling of levee breach including slumping failure of breach sides. Journal of Hydraulic Engineering 144(2): 04017066. doi: 10.1061/(ASCE)HY.1943-7900.0001406.

El kadi Abderrezzak, K., Die Moran, A., Mosselman, E., Bouchard, J. P., Habersack, H., Lebert, F., & Aelbrecht, D. (2014). A physical, movable-bed model for non-uniform sediment transport, fluvial erosion and bank failure in rivers. Journal of Hydro-environment Research 8(2): 95-114. doi: 10.1016/j.jher.2013.09.004.

El kadi Abderrezzak, K., Die Moran, A., Tassi, P., Ata, R., Hervouet, J. M. (2016). Modelling river bank erosion using a 2D depth-averaged numerical model of flow and non-cohesive, non-uniform sediment transport. Advances in Water Research, 93(A): 75-88. doi: 10.1016/j.advwatres.2015.11.004.

Frank, P.-J., & Hager, W. H. (2014). Spatial dike breach: Accuracy of photogrammetric measurement system. Proc. 7th International Conference on Fluvial Hydraulics (River Flow), Lausanne. doi: 10.1201/b17133-219.

Frank, P.-J., & Hager, W. H. (2015). Spatial dike breach: sediment surface topography using photogrammetry. Proc. 36th IAHR World Congres, The Hague.

Frank, P.-J (2016) Hydraulics of spatial dike breach, Dissertation, ETH of Zurich.

Frank, P.-J., & Hager, W. H. (2016). Challenges of dike breach hydraulics. Proc. 8th International Conference on Fluvial Hydraulics (River Flow), Saint Louis, Mo. doi: 10.1201/9781315644479-70.

Friedl, F., Schneider, J., Hinkelammert, F., & Weitbrecht, V. (2018). Through-water terrestrial laser scanning in hydraulic scale models: proof of concept. Journal of Hydraulic Research 56(4): 551-559. doi: 10.1080/00221686.2017.1372820.

Glassner, A. S. (1989) An Introduction to Ray tracing. Elsevier Science.

Henning, M., Hentschel, B., & Hüsener, T. (2008) Determination of channel morphology and flow features in laboratory models using 3D-photogrammetry. Proc. International Conference on Fluvial Hydraulics (River Flow), Izmir.

Hoshino, T., & Yasuda, H. (2015). 3D measurement of water and bed surface profiles during formation of sand waves with moving optical cutting method. Proc. 9th Symposium on River, Coastal and Estuarine Morphodynamic (RCEM), Iquitos.

Hung, C. Y., & Capart, H. (2013). Rotating laser scan method to measure the transient free-surface topography of small-scale debris flows. Experiments in Fluids 54:1455. doi: 10.1007/s00348-013-1544-0.

Jandora, J., & Ríha, J. (2008). The Failure of Embankment Dams Due to Overtopping. Vutium, ISBN 8021435275.

Kakinuma, T., & Shimizu, Y. (2014). Large-scale experiment and numerical modeling of a riverine levee breach. Journal of Hydraulic Engineering 140(9):1-9. doi: 10.1061/(ASCE)HY.1943-7900.0000902.

Lane, S. N. (2000). The Measurement of river channel morphology using digital photogrammetry. Photogrammetric Record 16(96): 937-961.

Marzan, G. T., & Karara, H. M. A. (1975). Computer program for direct linear transformation solution of the collinearity condition, and some applications of it. Proc. Symposium on Close-Range Photogrammetric Systems, Falls Church, VA.

Massot-Campos, M., & Oliver-Codina, G. (2015). Optical sensors and methods for underwater 3D reconstruction. Sensors 15(12): 31525-31557. doi: 10. 3390/s151229864.

Morasso, P., & Mohan, V. (2006). Summary of DLT method for stereo camera calibration, 3D Reconstruction and Robot-camera Integration. GNOSYS internal report.

Morgan, J. A., Brogan, D. J., & Nelson, P. A. (2017). Application of structure-from-motion photogrammetry in laboratory flumes. Geomorphology 276: 125-143. doi:10.1016/j. geomorph.2016.10.021.

Morris, M., Hassan, M., & Vaskinn, K. (2007). Breach formation: Field test and laboratory experiments. Journal of Hydraulic Research 45(sup1): 9-17. doi: 10.1080/00221686.2007.9521828.

Onda, S., Hosoda, T., Jaćimović, N. M., & Kimura, I. (2019). Numerical modelling of simultaneous overtopping and seepage flows with application to dike breaching. Journal of Hydraulic Research 57(1): 13-25. doi: 10.1080/00221686.2018.1442882.

Pickert, G., Jirka, G. H., Bieberstein, A., & Brauns, J. (2004). Water Interaction during the breaching process of overtopped embankments. Proc. 2nd International Conference on Fluvial Hydraulics (River Flow), Naples.

Pickert G, Weitbrecht V, & Bieberstein A. (2011) Breaching of overtopped river embankments controlled by apparent cohesion. Journal of Hydraulic Research 49(2): 143-156. doi: 10.1080/00221686.2011.552468.

Rifai, I., Erpicum, S., Archambeau, P., Violeau, D., Pirotton, M., Dewals, B., & El Kadi Abderrezzak, K. (2016). Sensitivity of the breaching process in the case of overtopping induced fluvial dike failure. Proc. 8th International Conference on Fluvial Hydraulics (River Flow), Saint Louis, Mo. doi: 10.1201/9781315644479-286.

Rifai, I., Erpicum, S., Archambeau, P., Violeau, D., Pirotton, M., El Kadi Abderrezzak, K., & Dewals, B. (2017). Overtopping induced failure of noncohesive, homogeneous fluvial dikes. Water Resources Research 53(4): 3373-3386. doi:10.1002/2016WR020053.

Rifai, I., El Kadi Abderrezzak, K., Erpicum, S., Archambeau, P., Violeau, D., Pirotton, M., & Dewals, B. (2018). Floodplain backwater effect on overtopping induced fluvial dike failure. Water Resources Research 54(11) 9060-9073. doi: 10.1029/2017WR022492.

Rifai, I., El Kadi Abderrezzak, K., Erpicum, S., Archambeau, P., Violeau, D., Pirotton, M., & Dewals, B. (2019a). Flow and detailed 3D morphodynamic data from laboratory experiments of fluvial dike breaching. Scientific Data 6:53. doi.org/10.1038/s41597-019-0057-y.

Rifai, I., El Kadi Abderrezzak, K., Erpicum, S., Archambeau, P., Violeau, D., Pirotton, M., & Dewals, B. (2019b). Accompanying dataset for: “Flow and detailed 3D morphodynamic data from laboratory experiments of fluvial dike breaching” Zenodo, https://doi.org/10.5281/zenodo.1494800 (2018).

Rifai I., El Kadi Abderrezzak, K., Hager, W.H., Erpicum, S., S., Archambeau, P., Violeau, D., Pirotton, M., 1 Dewals, B. (2020). Apparent cohesion effects on overtopping induced fluvial dike breaching. Journal of Hydraulic Research. doi: 10.1080/00221686.2020.1714760.

Schmocker, L. (2011). Hydraulics of Dike Breaching. Dissertation, ETH Zurich.

Schmocker, L., & Hager, W. H. (2009). Modelling dike breaching due to overtopping. Journal of Hydraulic Research 47(5): 585-597. doi:10.3826/jhr.2009.3586.

Schmocker, L., & Hager, W. H. (2012). Plane dike breaching due to overtopping: effects of sediment, dike height and discharge. Journal of Hydraulic Research 50(6): 576-586. doi: 10.1080/00221686.2012.713034.

Shimada, T., Hirai, Y. & Tsuji, T. (2010). Levee breach experiment by overflow at the Chiyoda Experimental Flume. Journal of Japan Society of Civil Engineers Ser. B1 (Hydraulic Engineering), 54: 811-816.

Smith, M. W., Vericat, D., & Gibbins, C. (2012). Through-water terrestrial laser scanning of gravel beds at the patch scale. Earth Surface Processes and Landforms 37(4): 411-421.doi: 10.1002/esp.2254.

Smith, M. W., & Vericat, D. (2014). Evaluating shallowwater bathymetry from through-water terrestrial laser scanning under a range of hydraulic and physical water quality conditions. River Research and Applications 30: 905-924. doi: 10.1002/rra.2687.

Soares-Frazão, S., Le Grelle, N., Spinewine, B., & Zech, Y. (2007). Dam-break induced morphological Changes in a channel with uniform sediments: Measurements by a Laser-sheet imaging technique. Journal of Hydraulic Research 45(Extra Issue):87-95. doi: 10.1080/00221686.2007.9521835.

Spinewine, B., Delobbe, A., Elslander, L., & Zech, Y. (2004). Experimental investigation of the breach growth process in sand dikes. Proc. 2nd International Conference on Fluvial Hydraulics (River Flow), Naples.

Tabrizi, A. A., Elalfy, E., LaRocque, L. A., Chaudhry, M. H, & Imran, J. (2015). Experimental modeling of levee failure process due to overtopping. Proc. Annual Meeting of Association of State Dam Safety Officials (ASDSO), New Orleans, LO.

Tal, M., Frey, P., Kim, W., Lajeunesse, E., Limare, A., & Métivier, F. (2012). The use of imagery in laboratory experiments. Fluvial Remote Sensing for Science and Management: 299-321. doi: 10.1002/9781119940791.ch13.

Tian, Q, Todd Lowe, K, & Simpson, R. L. A. (2010). Laser-based optical approach for measuring scour depth around hydraulic structures. Proc. 5th International Conference on Scour and Erosion, San Francisco, CA.

Younkin, B. D, & Hill, D. F. (2009). Rapid profiling of an evolving bed form using planar laser sheet illumination. Journal of Hydraulic Engineering 135: 52-56. doi: 10.1061/(ASCE)HY.1943-7900.0000085.

Volz, C., Frank, P.-J., Vetsch, D. F, Hager, W. H, & Boes, R. M. (2017). Numerical embankment breach modelling including seepage flow effects. Journal of Hydraulic Research 55(4): 480-490. doi: 10.1080/00221686.2012.732970.

Wallner, S. (2014). Influence of reservoir shape and size on the flood wave caused by progressive overtopping dam failure. Dissertation, TU Wien.

Walton; J. S. (1981). Close-range Cine-photogrammetry: a generalized technique for quantifying gross human motion. Dissertation, Pennsylvania State University.